Comparing Resource Adequacy Metrics and their Influence on Capacity Value

Eduardo Ibanez and Michael Milligan
Transmission and Grid Integration Group
National Renewable Energy Laboratory
Golden, CO USA
eduardo.ibanez@nrel.gov, michael.milligan@nrel.gov

***Abstract*—Traditional probabilistic methods have been used to evaluate resource adequacy. The increasing presence of variable renewable generation in power systems presents a challenge to these methods because, unlike thermal units, variable renewable generation levels change over time because they are driven by meteorological events. Thus, capacity value calculations for these resources are often performed to simple rules of thumb. This paper follows the recommendations of the North American Electric Reliability Corporation's Integration of Variable Generation Task Force to include variable generation in the calculation of resource adequacy and compares different reliability metrics. Examples are provided using the Western Interconnection footprint under different variable generation penetrations.**

***Index Terms*—Capacity planning, power system reliability, probability, solar energy, wind energy**

I. Introduction

The increasing amount of electrical load served by variable generation (VG) such as wind and solar photovoltaic energy in the United States and many other countries has stimulated an interesting line of research to better quantify the capacity value of these resources. Traditional methods applied to thermal units based on their nominal capacity and average outage rates do not apply to VG because of their variable, uncertain, and nondispatchable nature. The North American Electric Reliability Corporation's Integration of Variable Generation Task Force recently released a report that highlighted the need to develop and benchmark metrics that reasonably and fairly calculate the capacity value of solar and wind power [1]. As the fraction of generation coming from VG becomes more relevant, the estimated capacity value of VG will have an impact on system planning [2]. However, many system operators ignore VG capacity value or base their estimations on simple rules of thumb, such as a nominal and predetermined value or an average of certain hours of the year [3].

This work was supported by the U.S. Department of Energy under Contract No. DE-AC36-08-GO28308 with the National Renewable Energy Laboratory.

In this paper, we provide a method to include VG in traditional, probabilistic-based, adequacy methods. This method has been implemented in the Renewable Energy Probabilistic Resource Adequacy (REPRA) tool. The tool is used to compare different metrics to quantify system risk. The methodology is applied to different renewable penetrations in the U.S. Western Interconnection.

The remainder of the paper is organized as follows: Section II introduces the concept of effective load-carrying capability; Section III describes the proposed modeling framework; Section IV describes the numerical example; Section V summarizes results and findings; and, finally, Section VI concludes.

II. Resource Adequacy and Probabilistic Metrics

Generation system adequacy is the subset of electrical system adequacy/reliability that ensures that available capacity is sufficient to meet expected demand within an acceptable risk threshold [4] at some future date in the planning horizon. The metrics most commonly used to assess system adequacy revolve around the loss-of-load probability (LOLP). The loss-of-load expectation (LOLE) is a measurement of the expected days in a year that could face a generation shortfall. Similarly, the loss-of-load hours (LOLH) measures the expected number of hours in a year with insufficient generation. Expected unserved energy (EUE) provides an estimation of the energy not likely to be served with the proposed generation portfolio. The current standard practice in the industry is to consider a LOLE level of 1 day in 10 years as an acceptable target. This paper compares this metric and level to other alternatives.

The literature review in [5] and more-recent examples in [1] and [6] present the effective load-carrying capability (ELCC) as an emerging suitable metric to evaluate the capacity value of VG. Given a reliability target, ELCC is defined as the maximum load that could be served by a system while meeting said reliability target. The ELCC can also be defined for a single generation unit as the increase in the system ELCC when that unit is added to the system [7]. Fig. 1 shows a graphical representation of this definition. The red horizontal line represents the reliability target of 1 day in 10

years, which is a common target used in the industry. The blue line represents the reliability curve for the units already in the system, which has an ELCC of 10 GW. When a new generation unit is added, the reliability curve shifts to the right. The horizontal difference between the system curves, 400 MW, represents the new unit's ELCC. The example shows the addition of wind generation, but the principle applies to any type of resource. The fraction of ELCC to installed capacity is generally close to one for conventional generation and significantly less for wind generation. Solar power capacity values calculated by this method are generally higher than wind resources but lower than conventional generation.

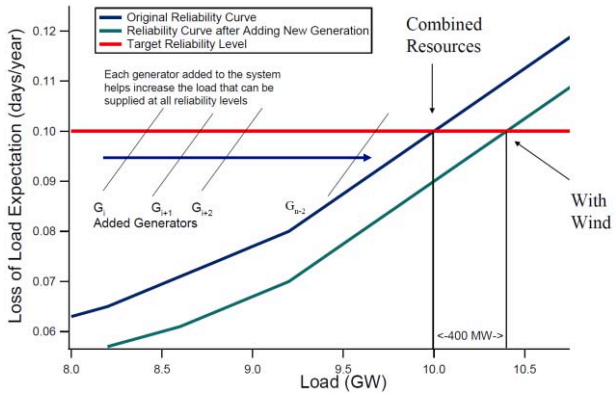

Figure 1. The unit ELCC is the horizontal distance between the reliability curves, measured at the target reliability level (400 MW at 1 day/10 years).

This value is also referred to as the capacity value (or credit) of the unit, because it measures the portion of the unit's nominal capacity that contributes to the system during the most critical hours. Although the choice of reliability target can change the ELCC and capacity value results (by performing the calculations in different areas along the reliability curve), the results section suggests that this effect is moderate over a wide range of targets.

This methodology can also be used to estimate the contribution of higher levels of transmission in interconnected systems. Analytical examples available in the literature are limited to two or three interconnected areas [4,8]. Alternative methodologies include the use of Monte Carlo simulations, e.g., in GE's Multi-Area Reliability Simulation program [9] or combined with decomposition methods [10].

III. THE REPRA TOOL

The REPRA tool is being developed at the National Renewable Energy Laboratory to better understand how different generation types can contribute to the resource adequacy of the power system from a reliability point of view. The different types include renewable generation, which are usually nondispatchable sources of power. At the core of the model resides a fast-convolution algorithm that combines the probability distribution of the traditional generators. These are represented by a finite number of states. The simplest case is modeled with a Bernoulli distribution, with a probability that each unit is not available equal to its equivalent forced outage rate, that is:

$$P(x) = \begin{cases} EFOR, & x = 0 \\ (1 - EFOR), & 0 < x \leq C \\ 0, & x > C \end{cases} \quad (1)$$

where C is the unit's capacity, x is the generation level, and $P(x)$ is the probability associated with that generation level.

The probability of multiple units is combined in a process known as convolution [3]. A very simple method to examine the combined probability is through the use of a capacity outage probability table, which indicates the LOLP for all levels of load the system can serve.

Unlike traditional generators, VG production is not solely limited by the nameplate capacity but also by the available driving resources such as wind speed or solar irradiance, which are governed by weather patterns. These patterns usually fluctuate and follow daily and seasonal trends. To preserve this variation, we make use of a sliding-window technique [11] for all hours of the year. Fig. 2 shows a graphical representation of a sliding window, which includes the current and adjacent hours. The width is predetermined but adjustable; in this case, it includes a total of five hours, but can also be modified to include adjacent days. Power outputs in the window are combined with probabilities (in this case, they are equal) to create a probability distribution similar to that showed in (1). For each hour of the year, this distribution can be convolved with the thermal outage table.

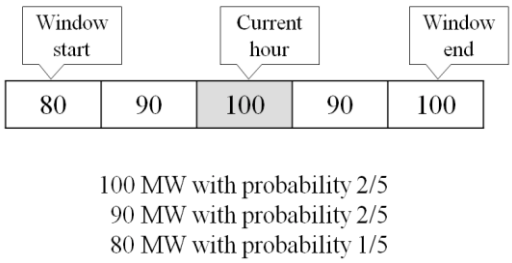

Figure 2. Example of a sliding window for wind power generation

IV. NUMERICAL EXAMPLE

In this section, we apply the reliability tool introduced in the previous section to the U.S. Western Interconnection footprint. The representation of the generation fleet is based on the National Renewable Energy Laboratory's Western Wind and Solar Integration Study Phase 2 (WWSIS-2) [12]. This data is consistent with other studies performed by the Western Electricity Coordinating Council's Transmission Expansion Planning Policy Committee [13].

Table I contains the list of balancing authority areas (BAAs) that are considered in this example. BAAs are grouped into eight subregions, following the suggested zones in [14]. Fig. 3 presents a map of the different BAAs and the subregions to which they belong, which are differentiated by shades. Throughout this paper, WAUW is merged with NWMT because of the small size of the former.

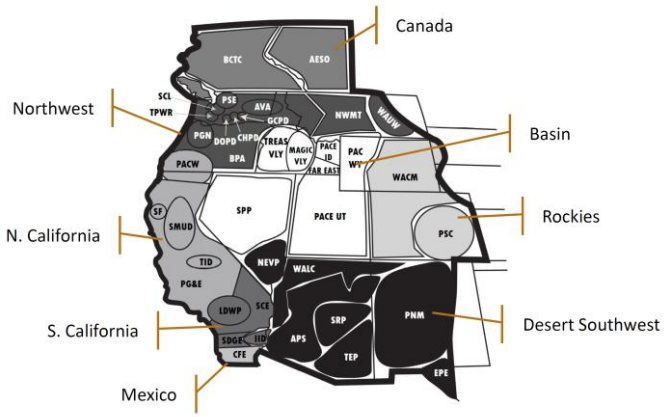

Figure 3. Western Electricity Coordinating Council BAAs and subregions

TABLE I. BAAS AND SUBREGIONS IN THE WESTERN ELECTRICITY COORDINATING COUNCIL

Subregion	Code	Balancing Authority Area
Northwest	AVA	Avista
	BPA	Bonneville Power Administration
	CHPD	PUD No. 1 of Chelan County
	DODP	PUD No. 1 of Douglas County
	GCPD	PUD No. 1 of Grant County
	NWMT	Northwest Energy
	PGN	Portland General Electric
	PSE	Puget Sound Energy
	SCL	Seattle City Light
	TPWR	Tacoma Power
	WAUW	WAPA – Upper Great Plains West
Northern California	PACW	PacifiCorp West
	PG&E	Pacific Gas and Electric
	SMUD	Sacramento Municipal Utility District
	TID	Turlock Irrigation District
Southern California	IID	Imperial Irrigation District
	LDWP	LA Dpt. of Water and Power
	SCE	Southern California Edison
	SDGE	San Diego Gas and Electric
Basin	FAR EAST	Far East
Basin	FAR EAST	Far East
	MAGIC VLY	Magic Valley
	PACE ID	PacifiCorp East (Idaho)
	PACE UT	PacifiCorp East (Utah)
	PACE WY	PacifiCorp East (Wyoming)
	SPP	Sierra Pacific Power (NV Energy)
	TREAS VLY	Treasure Valley
Rockies	PSC	Public Service Company of Colorado
	WACM	WAPA – Colorado Missouri Region
Desert Southwest	APS	Arizona Public Service
	EPE	El Paso Electric
	NEVP	Nevada Power
	PNM	Public Service Company of New Mexico
	SRP	Salt River Project
	TEP	Tucson Electric Power
	WALC	WAPA – Lower Colorado Region
Canada	AESO	Alberta
	BCTC	British Columbia Transmission Corp.
Mexico	CFE	Comisión Federal de Electricidad

WWSIS-2 examined the effect of integrating large amounts of renewable energy into the Western Interconnection by studying three scenarios with 33% renewable energy penetration and a reference scenario based on [13]. Table II summarizes the breakdown of wind and solar power for these scenarios. Even though the Base and High Solar scenarios have the same wind power penetration, the siting of the wind is different, thus the necessary capacity to achieve the 8% energy penetration leads to slightly different amounts of installed capacity. Although solar power refers to both photovoltaic and concentrating solar power, only photovoltaic was considered in this analysis. This is because concentrating solar power in WWSIS-2 was assumed to have several hours of storage built-in, thus making it dispatchable to a certain degree. Calculation of capacity value with storage is another current field of research [15].

TABLE II. WESTERN WIND AND SOLAR INTEGRATION STUDY PHASE 2 SCENARIOS

Scenario	Wind Penetration	Solar Penetration	Wind Capacity (GW)	Solar Capacity (GW)
Base	8%	3%	27.9	11.4
High Wind	25%	8%	66.2	34.6
High Mix	16.5%	16.5%	43.8	54.9
High Solar	8%	25%	23.4	81.7

Load time series data from 2006 was chosen from the Ventyx Velocity Suite [16] and were increased to represent the load in 2020, the focus year. The wind data set was derived from the large wind speed and power database [17] developed by 3TIER using a numerical weather prediction model applied to the Western United States. Because the model allows for the re-creation of the weather at any time and space, wind speed data was sampled at representative hub heights for modern wind turbines every 10 minutes during a 3-year period on a 2-km spatial resolution. The resulting data set was then used to construct the 2006 time series, which was paired with the 2006 load data time series to preserve the consistency of common weather impacts. Solar data was produced by the National Renewable Energy Laboratory [18] based on the satellite-derived irradiance generated by the State University of New York/Clean Power Research [19], which is available on a 10-km grid at an hourly resolution.

V. RESULTS

A. *Metric Comparison*

ELCC values are calculated at the BAA, subregion, and interconnection levels following the structure in Table I. LOLE is used as the driving metric for the calculations for a wide range of values (from 1 day in 1 year to 1 day in 100 years) in this section. The LOLH and EUE metrics are calculated for each case. This section summarizes the observed relationships.

For all the footprints, we find that the behavior between the three metrics resembles a linear relationship, especially between LOLE and LOLH. Figs. 4 and 5 show examples of these relationships.

The slopes shown in Figs. 4 and 5 vary significantly across the different regions. To better understand the origin of these slope changes for the LOLE and LOLH cases, we utilize Fig. 6, which represents the top 25 hours in decreasing LOLP order. All the hours contribute to the LOLH metric; whereas

only a few hours contribute to the LOLE metric (the largest value per day, highlighted in red). Fig. 6 reveals that the areas with the smallest slope are those that have very sharp decline in LOLP value and, as a result, have very few hours that contribute mostly to both LOLH and LOLE. Alternatively, more evenly distributed LOLP curves result in high LOLH-to-LOLE ratios.

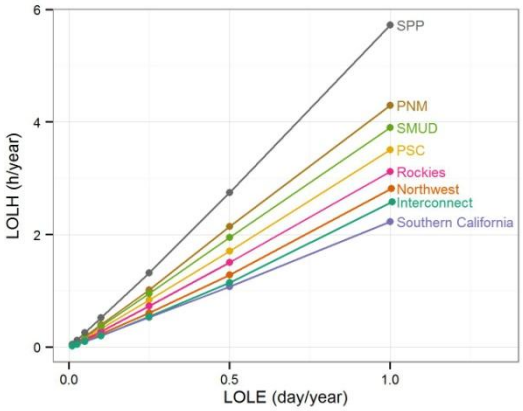

Figure 4. LOLH versus LOLE for the selected BAAs, subregions, and the Western Interconnection

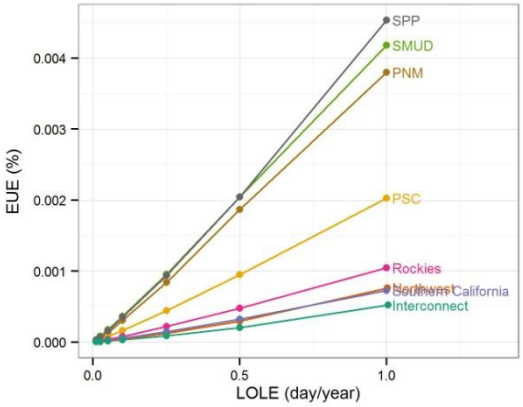

Figure 5. EUE versus LOLE for the selected BAs, subregions, and the Westner Interconnection

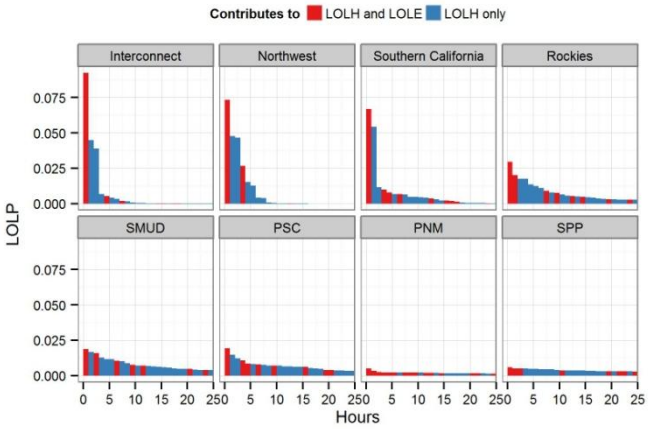

Figure 6. LOLP for the top 25 hours for 0.1 day/year for the selected BAAs, subregions, and the Westner Interconnection

This behavior is driven mainly by two factors: net load distributions and the probabilistic convolution of traditional generators. Fig. 7 summarizes the 25 top net load hours, which coincide with the same hours in Fig. 6. Large drops between the first top hours tend to create small LOLH-to-LOLE ratios, e.g., Southern California of the Western Interconnection. The sharp decrease is not sufficient to guarantee that behavior, as is the case for PNM. The translation between demand levels and LOLP depends on the convolution of the generating units. Fig. 8 shows that these curves can vary significantly, especially for smaller footprints with fewer generators.

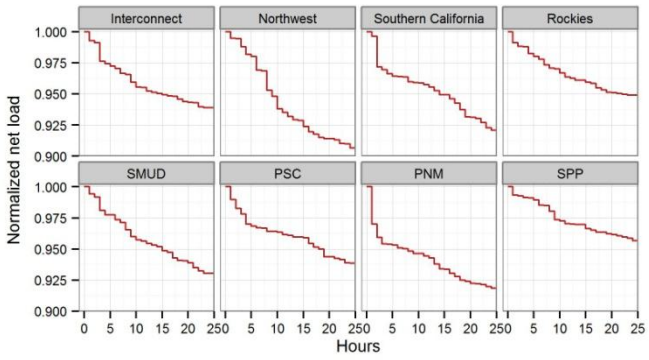

Figure 7. Net load duration curves for 1 d/10 years LOLE level for the selected BAAs, subregions, and the Western Interconnection

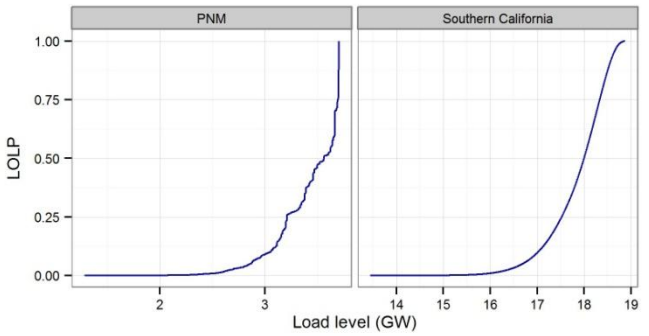

Figure 8. LOLP versus load level for two subregions

The linear relationship between LOLE and LOLH can be studied through the graphs in Figs. 9 and 10 (Interconnect and PSC, respectively). Using the same coloring scheme to discern the top 25 hours that contribute to LOLE and LOLH, different LOLE target cases are represented. In both figures, even though the magnitudes of LOLP change, the relative shape of the distribution remains fairly stable. Thus, the LOLH-to-LOLE ratios remain close to constant for the cases observed.

A similar process can be followed to explain the relationship between LOLE and EUE. In this case, one needs to compare the LOLP of the top hours by day to the EUE of the individual hours. There are instances in which the behavior does not adjust as well to a linear relationship because of the necessary translation between LOLP and EUE, as shown in Fig. 11.

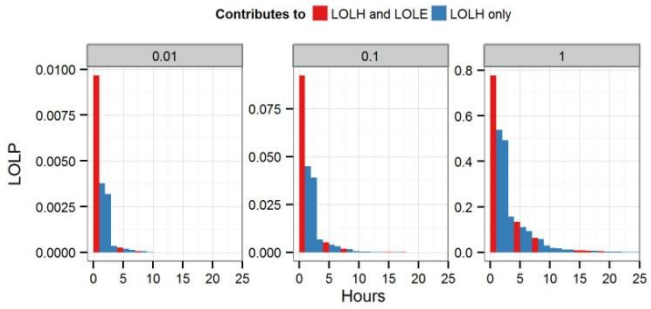

Figure 9. LOLP for the top 25 hours for different LOLE targets for the Western Interconnection

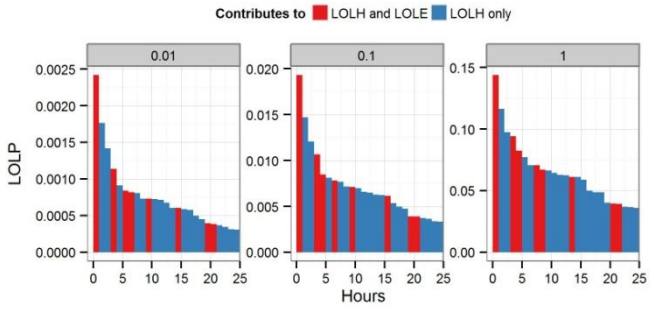

Figure 10. LOLP for the top 25 hours for different LOLE targets for PSC

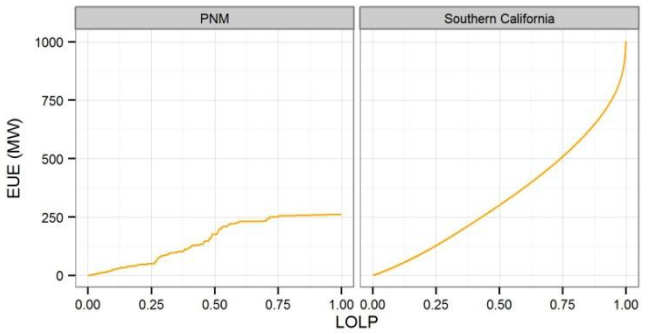

Figure 11. The relationship between LOLP and EUE

B. *Effect on Capacity Value*

After understanding the behavior of the different metrics, we proceed to estimate their effect on capacity value. To do this, ELCC values are calculated for the system with and without VG. The different metrics are used, making sure that they are consistent across different reliability levels. For instance, after calculating ELCC using an LOLE of 1 day in 10 years, the observed values for LOLH for that case are annotated. Then ELCC calculations are performed with and without VG achieving the desired LOLH level. The capacity value calculated by both methods is done under equivalent levels of reliability.

Fig. 12 shows the reliability curves (first suggested in Fig. 1) for different metrics. These curves are depicted for four scenarios: conventional generation only, with wind, with photovoltaic, and with the addition of both.

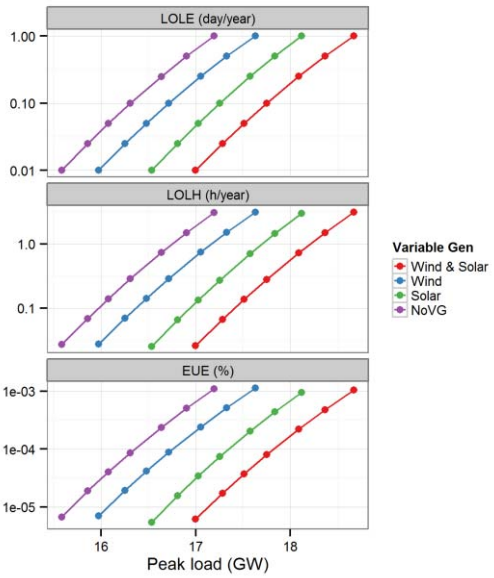

Figure 12. Different metrics versus peak load (or ELCC) for PSC

It is not surprising to see that the curves behave similarly given the underlying linear relationship between metrics. As mentioned earlier, capacity value can then be calculated by measuring the horizontal distance between two curves. These are calculated for all the areas and different equivalent levels of reliability. Fig. 13 shows the results across all deployment scenarios for the Rockies and Southern California subregions. According to the results, capacity value is rather insensitive to metric selection. This is not surprising after understanding the tight relationships between the metrics. Further, the reliability level targeted is very small, especially given that the results expand two orders of magnitude.

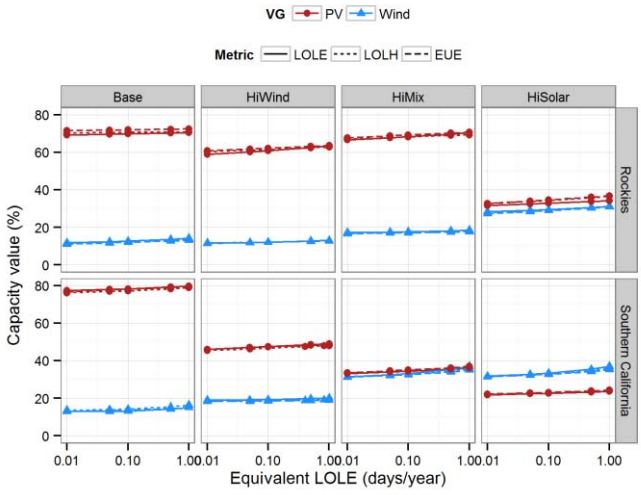

Figure 13. Wind and photovoltaic capacity value for the Rockies and Southern California by metrics and WWSIS-2 scenario

VI. CONCLUSIONS

The paper presents a methodology to include VG in traditional resource adequacy calculations. Different metrics

based on the concept of ELCC are presented and compared through a numerical example that expands a multitude of regions in the Western Interconnection and for different levels of wind and solar penetration.

The comparison of metrics suggests an underlying linear relationship between them, and these patterns are explained by studying the different cases. VG capacity values are calculated with the alternative metrics and compared for equivalent reliability levels, and they are found to be rather close. Similarly, the reliability level chosen does not have a significant impact on the capacity value calculations. Future work will examine these findings for other footprints and years of data and will consider whether the definition of the metrics is responsible for the observed results from a theoretical point of view.

REFERENCES

[1] Integration of Variable Generation Task Force, "Methods to model and calculate capacity contributions of variable generation for resource adequacy planning," North American Electric Reliability Corporation, Princeton, NJ, , Rep., 2011 [Online]. Available: http://www.nerc.com/docs/pc/ivgtf/IVGTF1-2.pdf

[2] M. Milligan and K. Porter, "Wind capacity credit in the United States," in *Proc. 2008 IEEE PES GM*, pp. 1–5.

[3] J. Rogers and K. Porter, "Summary of time period-based and other approximation methods for determining the capacity value of wind and solar in the United States: September 2010–February 2012," National Renewable Energy Laboratory, Golden, CO, Subcontract Rep. NREL/SR-5500-54338, 2012 [Online]. Available: http://www.nrel.gov/docs/fy12osti/54338.pdf

[4] R. Billinton and R. N. Allan, *Reliability Evaluation of Power Systems*, New York: Plenum Press, 1996.

[5] M. Milligan and K. Porter, "Determining the capacity value of wind: An updated survey of methods and implementation," presented at WindPower, Houston, TX, 2008 [Online]. Available: http://www.nrel.gov/docs/fy08osti/43433.pdf

[6] A. Keane, M. Milligan, C. J. Dent, B. Hasche, C. D'Annunzio, K. Dragoon, H. Holttinen, N. Samaan, L. Soder, and M. A. O'Malley, "Capacity value of wind power," *IEEE Trans. on Power Syst.*, vol. 26, no. 2, pp. 564–572, May 2011.

[7] L. L. Garver, "Effective Load Carrying Capability of Generating Units," *IEEE Trans. Power Syst.*, vol. PAS-85, no. 8, pp. 910-919, Aug. 1966.

[8] L. Goel, C. K. Wong, and G. S. Wee, "And educational software package for reliability evaluation of interconnected systems," *IEEE Trans. on Power Syst.*, vol. 10, no. 3, pp. 1,147–1,153, Aug. 1995.

[9] G. E. Haringa, G. A. Jordan, and L. L. Garver, "Application of Monte Carlo simulation to multi-area reliability evaluation," *IEEE Computer Applications in Power*, vol. 4, pp. 21–25, Jan. 1991.

[10] B. Hasche, M. Wattiau, K. Grave, and R. Kuwahata, "Generation system adequacy in Europe: Application of a multi-area reliability calculation," presented at the 11th Annual Int. Workshop on Large-Scale Integration of Wind Power into Power Systems as Well as on Transmission Networks for Offshore Wind Power Plants, Lisbon, Portugal, Oct. 2012.

[11] M. Milligan, "A chronological reliability model incorporating wind rorecasts to assess wind plant reserve allocation," presented at WindPower, Portland, OR, 2002 [Online]. Available: http://www.nrel.gov/docs/fy02osti/32210.pdf

[12] D. Lew, G. Brinkman, E. Ibanez, B. M. Hodge, M. Hummon, A. Florita, and M. Heaney, "The western wind and solar integration study phase 2," National Renewable Energy Laboratory, Golden, CO, Tech. Rep. NREL/TP-5500-55588, 2013 [Online]. Available: http://www.nrel.gov/docs/fy13osti/55588.pdf

[13] Transmission Expansion Planning Policy Committee Western Electricity Coordinating Council, "TEPPC 2020 study report–2010 study program: 10-year regional transmission plan," Western Electricity Coordinating Council, Salt Lake City, UT, Rep., Sept. 2011 [Online]. Available: http://www.wecc.biz/library/StudyReport/Documents/2020%20Study%20Report.pdf

[14] Western Electricity Coordinating Council, "2010 power supply assessment," Salt Lake City, UT, Rep. [Online]. Available: http://www.wecc.biz/Planning/ResourceAdequacy/PSA/

[15] S. H. Madaeni, R. Sioshansi, and P. Denholm, "Estimating the Capacity value of concentrating solar power plants with thermal energy storage: A case study of the southwestern United States," *IEEE Trans. on Power Syst.*, vol. 28, no. 2, pp.1,205–1,215, May 2013.

[16] Ventyx, "Energy market data,." Rep., 2010 [Online]. Available: http://www.ventyx.com/velocity/energy-market-data.asp

[17] 3TIER, "Development of regional wind resource and wind plant output datasets," National Renewable Energy Laboratory, Golden, CO, Subcontract Rep. NREL/SR-550-47676, 2010 [Online]. Available: http://www.nrel.gov/docs/fy10osti/47676.pdf

[18] K. Orwig, M. Hummon, B.-M. Hodge, and D. Lew, "Solar data inputs for integration and transmission planning studies," presented at the 1st Int. Workshop on Integration of Solar Power into Power Systems, Aarhus, Denmark, Oct. 2011.

[19] S. Wilcox, M. Anderberg, R. George, W. Marion, D. Myers, D. Renne, N. Lott, T. Whitehurst, W. Beckman, C. Gueymard, R. Perez, P. Stackhouse, and F. Vignola, "Completing production of the updated National Solar Radiation Database for the United States," presented at the Solar 2007 Conf., Cleveland, OH, July.